Tribology Letters (2023) 71:19
https://doi.org/10.1007/s11249-022-01688-y

ORIGINAL PAPER

Influence of Surface Roughness on Press Fits

B. N. J. Persson[1,2]

Received: 29 October 2022 / Accepted: 13 December 2022 / Published online: 28 December 2022
© The Author(s) 2022

Abstract
A press fit, also known as interference fit or friction fit, is a form of fastening between two tight fitting mating parts (usually two bodies with cylinder or conical surfaces) that produces a joint which is held together by friction after the parts are pushed together. I discuss the influence of surface roughness on the design of press fits. This topic has been addressed in the engineering community but only on an empirical level without a scientific backup. Here, I will apply the Persson contact mechanics theory to show how to include the surface roughness in the design criteria. I argue that one should use what I denote as the cylinder "stylus width" rather than the "caliper width" when determining the influence of the surface roughness of the compression (also denoted as the interference). In the classical approach using the caliper width, the compression is assumed to be independent of the elastic properties of the solids, but in the more accurate approach presented here using the stylus width the compression depends on the elastic properties and on the surface roughness power spectra of the involved solids. A detailed discussion of the relation between the root-mean-square roughness amplitude h_{rms} and the maximum asperity height $h_{\max}$, of interest in its own right, is also presented as it is needed for determining the relation between the stylus and caliper derived compression's.

Graphical Abstract

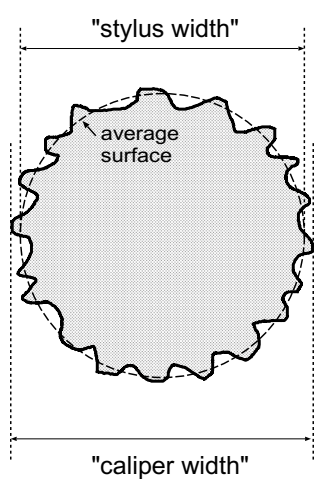

Keywords Surface roughness · Press fit · Compression · Stylus · Caliper

✉ B. N. J. Persson
b.persson@fz-juelich.de

1 Peter Grünberg Institute (PGI-1), Forschungszentrum Jülich, 52425 Jülich, Germany

2 Multiscale Consulting, Wolfshovener Str. 2, 52428 Jülich, Germany

1 Introduction

Press fit joints are commonly used in engineering constructions for connecting a shaft with a hub. Here we consider a hollow cylinder to be inserted in another hollow cylinder, see Fig. 1. The bigger cylinder (hub) has the outer and

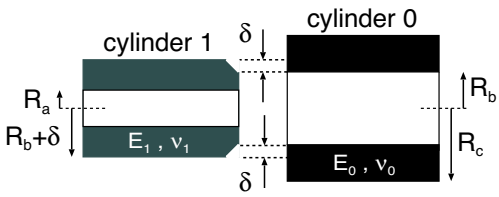

Fig. 1 The small cylinder 1 has an outer radius $R_b + \delta$ which is larger than the inner radius R_b of the bigger cylinder 0. The small cylinder can be inserted in the bigger one with an external force, or by cooling the small cylinder and heating the big cylinder so the thermal contraction of the small cylinder and thermal expansions of the big cylinder changes the dimensions so that the cylinders to be joined together without an external force (Color figure online)

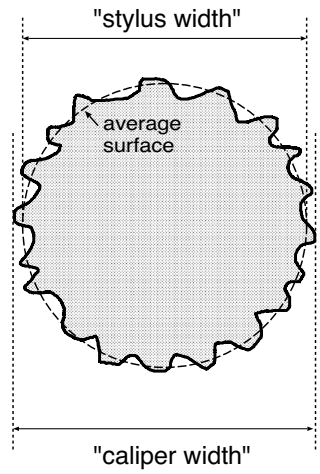

Fig. 2 The diameter of a cylinder with surface roughness depends on the experimental method used to determine it. A caliper will measure the distance between the top of the asperities in the cylinder-caliper contact areas, while using an engineering stylus the diameter of the dashed circular line (mean cylinder surface) can be ordained by fitting the measured height profile to a circle

inner radius R_c and R_b, and Young's modulus and Poisson ratio E_0 and ν_0, respectively. The smaller cylinder (shaft) has the outer and inner radius $R_b + \delta$ and R_a, respectively, and Young's modulus and Poisson ratio E_1 and ν_1, respectively (see Fig. 1). Here δ is denoted as compression distance or simply compression (also denoted interference) and we assume $\delta << R_b$.

Depending on the amount of compression, parts may be joined using a tap from a hammer or pressed together using a hydraulic ram. The inner cylinder may also be cooled and the outer cylinder heated before joining the parts. This result in a reduction of the outer radius of inner cylinder and an increase in the inner radius of the outer cylinder before fitting. This method allows the components to be joined without force and producing a fit compression when the components returns to normal temperature.

The force to separate the cylinders (pull-out force) depends on the compression, the friction coefficient, and the operating temperature. To maximize the pull-out force the highest allowable compression without yielding should be used. It is important to remember that differences in the coefficient of thermal expansion between the shaft and hub, especially when one is metal, can greatly reduce the compression. Therefore, changes in the operating temperature can lead to reductions in the compression and pull-out force. Note that press fits can only be used for materials which exhibit negligible creep. Thus it cannot be used for polymers, but most metals and ceramic materials exhibit negligible creep at room temperature.

One important application of press fit is in the reconstruction of hip joints. The engineers at various medical device companies chose to roughen the tapers for the hip implants. The idea was to soften the engagement so that they did not explode the ceramic femoral components but it led to an unfortunate softening of the taper, which led to fretting wear and corrosion. Many studies have been presented which shows how variability in stem taper surface topography affects the degree of corrosion and fretting in total hip arthroplasty [1, 2].

Other more standard applications where press fits are used for joining mechanical components are gear wheels on shafts, bearings on shafts and bearings in housings. The main advantages is that no fasteners are required, and that the joints are not permanent but can be disassembled and reassembled facilitating repair or replacement of parts.

In this communication I will discuss the influence of surface roughness on the design of press fits. This topic has been addressed in the engineering community, but only on an empirical level without a scientific backup [3–6]. Here I will apply the Persson contact mechanics theory and show how to include the surface roughness in the design criteria. In this study I neglect plastic deformations but for metals this can be included approximately on both the asperity level [7, 8] and on the macroscopic level [4, 5] using results presented elsewhere.

2 The Radius of Curvature and the Effective Compression δ_{eff}

There are essentially two different ways to measure the diameter of a cylinder. The simplest and standard way is to use a caliper. However, the caliper will measure the distance between the top of the highest asperities on the two sides of

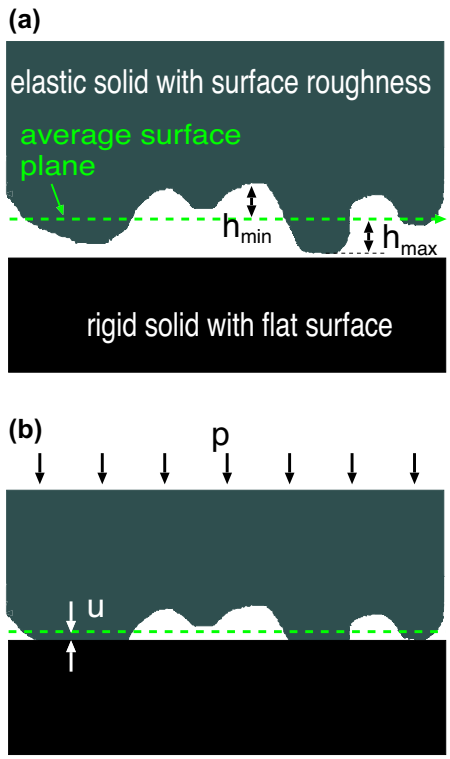

Fig. 3 **a** An elastic solid with surface roughness before contact with a rigid solid with a flat surface. The height of the highest asperity and the depth of the deepest valley in the considered interfacial region are denoted by $h_{\max}$ and $h_{\min}$, respectively, and will in general increase the larger the studied surface region is. **b** When the two solids are squeezed together with a pressure p the average surface separation will be u and will decrease as p increases. The empty volume between the solids is given by $V = A_0 u$ where A_0 is the nominal contact area (Color figure online)

the cylinder in a small area where the caliper makes contact with the cylinder. This will not give the separation between the average surface plane (dashed circular line in Fig. 2) on the two opposite sides of the cylinder. We will denote the compression obtained this way with δ_{caliper}. Another way to determine the effective diameter of the cylinder is to use an engineering stylus instrument to measure the surface topography in a circular segment in the angular direction. Fitting this to a circle (or cylinder) segment gives the radius of the dashed circular line in Fig. 2. We will denote the corresponding compression with δ_{stylus}.

When the cylinder surfaces have surface roughness, which is always the case, there will be a finite average surface separation at the interface (see Fig. 3b) which will result in a higher contact pressure than expected for smooth surfaces. In this case if $\delta = \delta_{\text{stylus}}$ then the compression δ to be used when calculating the contact pressure p is $\delta_{\text{eff}} = \delta_{\text{stylus}} + u$, where u is the average surface separation at the contacting interface $r = R_{\text{b}}$ (see Fig. 3b). For perfectly smooth surfaces $u = 0$ but in many applications u is comparable to δ.

In the engineering applications one usually measure the cylinder diameter with a caliper. In this case $\delta = \delta_{\text{caliper}} = \delta_{\text{stylus}} + h_{\max}$, where $h_{\max}$ is the height of the highest asperity above the average plane (dashed line in Fig. 3a) in the cylinder-caliper contact region, which typically is 3–5 times the root-mean-square (rms) roughness h_{rms} (see Sec. 3). Thus, in this case $\delta_{\text{eff}} = \delta_{\text{caliper}} - (h_{\max} - u)$.

In the engineering literature the "caliper-compression" is used when calculating the contact pressure. Thus, according to the DIN 7190 standard (see Ref. [6]) the effective compression to be used in calculations of the contact pressure is

$$\delta_{\text{eff}} = \delta_{\text{caliper}} - b(h_{z0} + h_{z1}), \tag{1}$$

where $b = 0.4$. Here, h_z is the sum of the height of the highest asperity and the deepest valley, $h_z = h_{\max} + h_{\min}$ (see Fig. 3). For a randomly rough surface, on the average $h_{\max} = h_{\min}$ and $h_z = 2h_{\max}$. We will discuss to what extent (1) holds in general. In order to do this we first need to discuss the statistical properties of randomly rough surfaces, a topic of interest in its own right.

3 Randomly Rough Surfaces

In the engineering approach to press fits, based on δ_{caliper}, enter $h_{\max}$ while in the approach I present below (based on δ_{stylus}) enter h_{rms}. Thus, to compare the two different approaches one need to know the relation between these quantities, which we will consider in this section for randomly rough surfaces.

All surfaces of solids have surface roughness, and many surfaces exhibit self-affine fractal behavior. This implies that if a surface area is magnified new (shorter wavelength) roughness is observed which appears very similar to the roughness observed at smaller magnification, assuming the vertical coordinate is scaled with an appropriate factor.

The roughness profile $z = h(\mathbf{x})$, where $\mathbf{x} = (x, y)$, of a surface can be written as a sum of plane waves $\exp(i\mathbf{q} \cdot \mathbf{x})$ with different wave vectors $\mathbf{q}$. The wavenumber $q = |\mathbf{q}| = 2\pi/\lambda$, where λ is the wavelength of one roughness component. The most important property of a rough surface is its power spectrum which can be written as

$$C(\mathbf{q}) = \frac{1}{(2\pi)^2} \int \mathrm{d}^2x \, \langle h(\mathbf{x}) h(\mathbf{0}) \rangle e^{i\mathbf{q}\cdot\mathbf{x}}, \tag{2}$$

where $\langle .. \rangle$ stands for ensemble averaging and where the integral is over the surface area. Assuming that the surface has isotropic statistical properties, $C(\mathbf{q})$ depends only on the magnitude q of the wave vector. A self affine fractal surface has a power spectrum $C(q) \sim q^{-2(1+H)}$ (where H is the Hurst exponent related to the fractal dimension $D_{\text{f}} = 3 - H$), which is a is a strait line with the slope $-2(1 + H)$ when

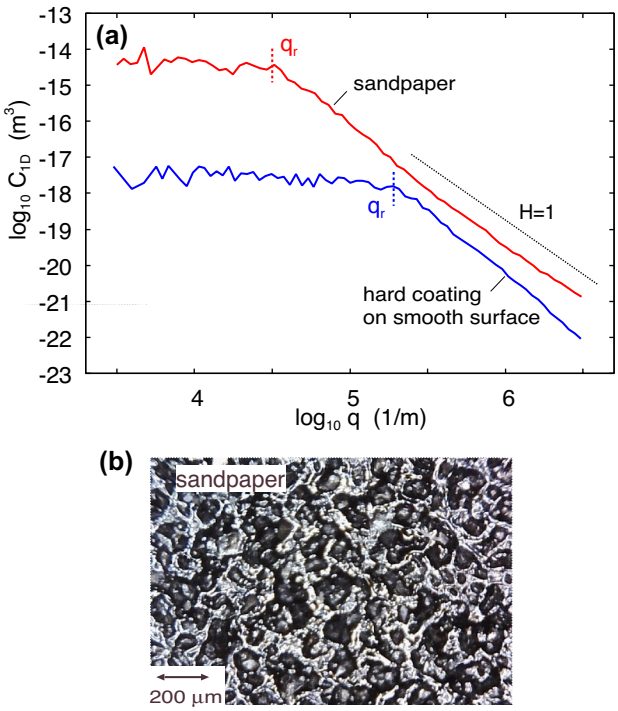

Fig. 4 **a** The 1D surface roughness power spectra as a function of the wave number (log-log-scale) for a sand paper grit 600 surface (red line) and for a hard coating on a smooth flat surface (blue line). The roll-off wavenumbers q_r are indicated. **b** An optical picture of the sand paper surface. The sand paper particles have the diameter $D \approx 20\,\mu$m but form structures (agglomerate of particles together with the glue) on the length scale $\lambda \approx 200\,\mu$m, giving the roll-off wavenumber $q_r = 2\pi/\lambda \approx 3 \times 10^4\ \mathrm{m}^{-1}$ indicated in the figure (Color figure online)

plotted on a log–log scale. Most solids have surface roughness with the Hurst exponent $0.7 < H < 1$ (see Ref. [9]).

For a one-dimensional (1D) line scan $z = h(x)$ the power spectrum is given by

$$C_{1D}(q) = \frac{1}{2\pi}\int_{-\infty}^{\infty} \mathrm{d}x\ \langle h(x)h(0)\rangle e^{iqx}. \tag{3}$$

For surfaces with isotropic roughness the 2D power spectrum $C(q)$ can be obtained directly from $C_{1D}(q)$ as described elsewhere [10–12].

For randomly rough surfaces, all the (ensemble averaged) information about the surface is contained in the power spectrum $C(\mathbf{q})$. For this reason the only information about the surface roughness which enter in contact mechanics theories (with or without adhesion) is the function $C(\mathbf{q})$. Thus, the (ensemble averaged) area of real contact, the interfacial stress distribution and the distribution of interfacial separations, are all determined by $C(\mathbf{q})$ [13–15].

Note that moments of the power spectrum determines standard quantities which are output of most topography instruments and often quoted. Thus, for example, the mean-square roughness amplitude

$$h_{\mathrm{rms}}^2 = \langle h^2\rangle = \int \mathrm{d}^2q\ C(\mathbf{q}), \tag{4}$$

and the mean-square slope

$$\xi^2 = \langle(\nabla h)^2\rangle = \int \mathrm{d}^2q\ q^2 C(\mathbf{q}), \tag{5}$$

are easily obtained as integrals involving $C(\mathbf{q})$. We will denote the root-mean-square (rms) roughness amplitude with h_{rms} and the rms slope with ξ. If $C(q)$ denote the angular average (in $\mathbf{q}$-space) of $C(\mathbf{q})$ then from (4):

$$h_{\mathrm{rms}}^2 = 2\pi\int_0^{\infty} \mathrm{d}q q\ C(q). \tag{6}$$

For isotropic roughness the 2D mean-square roughness amplitude is the same as the 1D mean-square roughness amplitude, but the mean-square slope is a factor of 2 larger in the 2D case.

Surfaces of bodies of engineering interest, e.g., a ball in a ball bearing or a cylinder in a combustion engine, have always a roll-off region for small wavenumbers q, because such bodies have some macroscopic shape, but are designed to be smooth at length scales smaller that the shape of the body (see Fig. 4 for two examples). In these cases the roll-off wavelength is determined by the machining process, e.g., by the size of the particles in sand paper or on a grinding wheel. If the roll-off region matters in a particular application depends on the size of the relevant or studied surface area. Thus, if the lateral size L is small the wavenumber $q = 2\pi/L$ may be so large that it will fall in the region where the surface roughness power spectrum exhibit self-affine fractal scaling, and the roll-off region will not matter. We note that some natural surfaces, such as surfaces produced by brittle fracture, have fractal-like roughness on all length scales up to the linear size of the body.

We will now discuss the relation between the height h_{max} of the highest asperity above the average surface plane and the rms roughness amplitude h_{rms}. No two surfaces have the same surface roughness, and h_{max} will depend on the surface used. To take this into account we have generated surfaces (with linear size L) with different random surface roughness but with the same surface roughness power spectrum. That is, we use different realizations of the surface roughness but with the same statistical properties. For each surface size we have generated 60 rough surfaces using different set of random numbers. The surface roughness was generated as described in Ref. [16] (appendix A) by adding plane waves

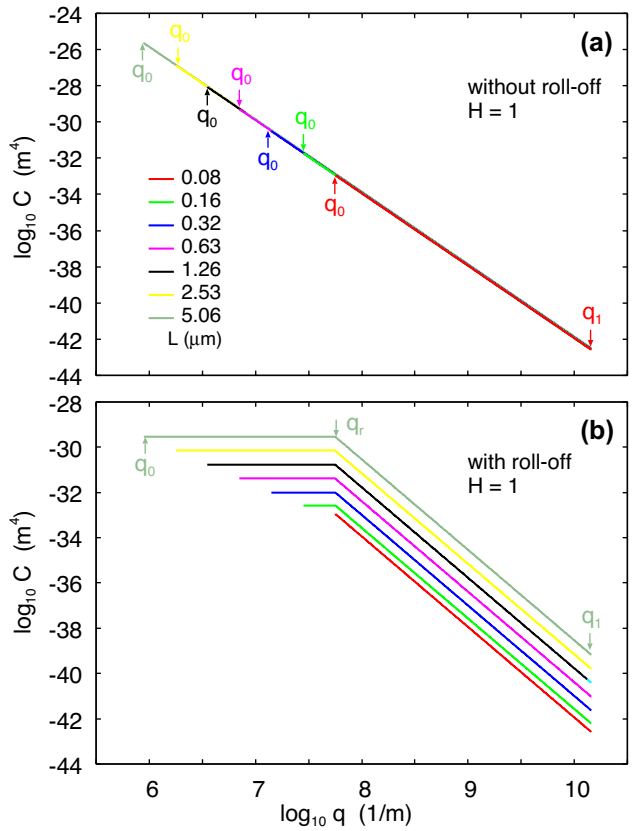

Fig. 5 The surface roughness power spectra as a function of the wave number (log-log-scale) used in the calculations of the surface height profile for surfaces with the Hurst exponent $H = 1$ without (**a**) and with (**b**) a roll-off region. In **a** we indicate the large and small wavenumber cut-off q_1 and q_0, and the **b** also the roll-off wavenumber q_r. For each system size $L = 2\pi/q_0$ the power spectra have been chosen so the rms roughness amplitude h_{rms} are the same with and without the roll-off region (Color figure online)

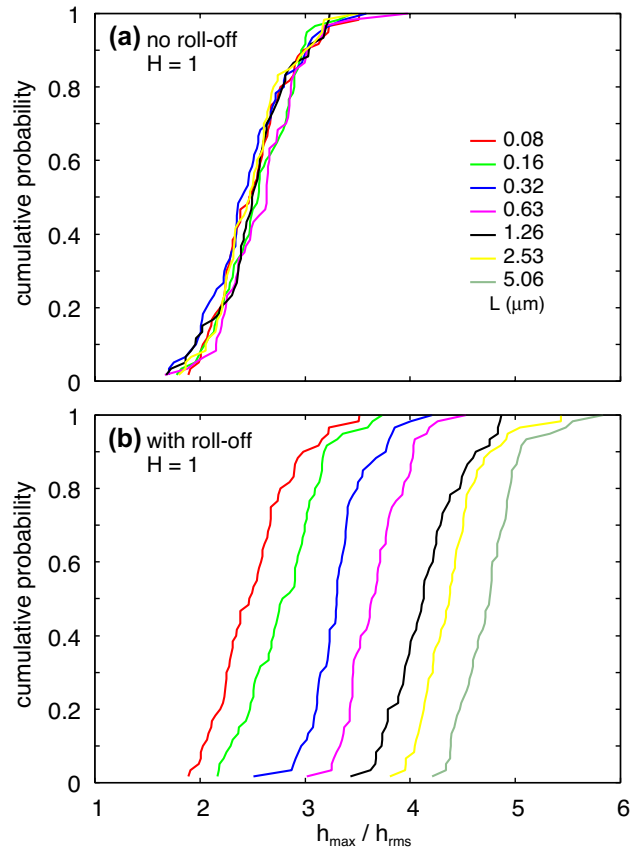

Fig. 6 The cumulative probability for the ratio h_{max}/h_{rms} between the height of the highest asperity (relative to the average surface plane) and the rms roughness amplitude for the power spectra shown in Fig. 5 without (**a**) and with (**b**) a roll-off region (Color figure online)

with random phases $\phi_{\mathbf{q}}$ and with the amplitudes determined by the power spectrum:

$$h(\mathbf{x}) = \sum_{\mathrm{q}} B_{\mathbf{q}} e^{i(\mathbf{q}\cdot\mathbf{x}+\phi_{\mathbf{q}})}, \tag{7}$$

where $B_{\mathbf{q}} = (2\pi/L)[C(\mathbf{q})]^{1/2}$. We assume isotropic roughness so $B_{\mathbf{q}}$ and $C(\mathbf{q})$ only depend on the magnitude of the wavevector $\mathbf{q}$.

We have used surfaces of square unit size, $L \times L$, with 7 different sizes, where L increasing in steps of a factor of 2 from $L = 79$ nm to $L = 5.06$ μm. The longest wavelength roughness which can occur on a surface with size L is $\lambda \approx L$ so when producing the roughness on a surface we only include the part of the power spectrum between $q_0 < q < q_1$ where $q_0 = 2\pi/L$ and where q_1 is a short distance cut-off corresponding to atomic dimension (we use

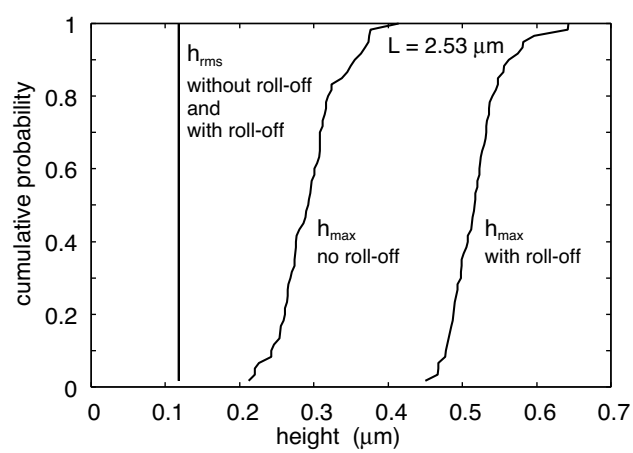

Fig. 7 The cumulative probability for the h_{max} and for h_{rms} for the power spectra shown in Fig. 5 without and with a roll-off region. For h_{rms} the results without and with a roll-off region overlap (note: the power spectra shown in Fig. 5 have been chosen so the rms roughness amplitude are the same with and without the roll-off region)

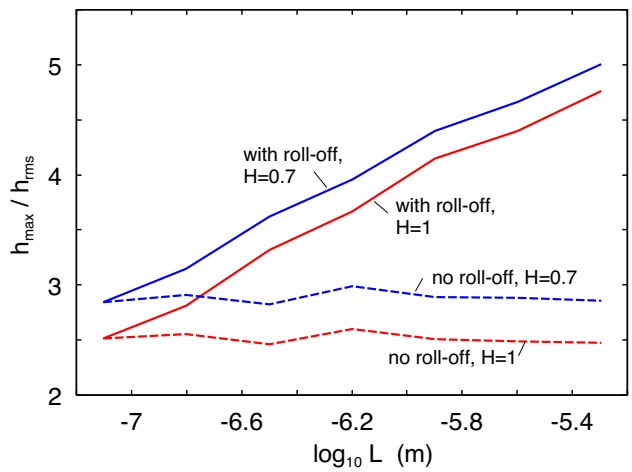

Fig. 8 The ratio h_{max}/h_{rms} between the height of the highest asperity (relative to the average surface plane) and the rms roughness amplitude for the power spectra shown in Fig. 5 ($H = 1$), and for similar power spectra for the Hurst exponent $H = 0.7$, as a function of the logarithm of the size of the unit L. The results are obtained after averaging over 60 realizations of the surface roughness (Color figure online)

$q_1 = 1.4 \times 10^{10}$ m^{-1}). This is illustrated in Fig. 5 which shows the different short wavenumber cut-off q_0 used.

We now study how the ratio h_{max}/h_{rms} depends on the surface roughness power spectra. We will consider two cases where there is (a) no roll-off region in the power spectra and (b) where a roll-off region occur. Figure 5 shows the surface roughness power spectra as a function of the wave number (log-log-scale) used in the calculations of the surface height profile for surfaces with the Hurst exponent $H = 1$ without (a) and with (b) a roll-off region. Note that a vertical shift in power spectra in (b) has no influence on the ratio h_{max}/h_{rms} since it correspond to scaling $C(\mathbf{q})$ with some factor s^2, which is equivalent to scaling $h(\mathbf{x})$ with the factor of s, which changes both h_{max} and h_{rms} with the same factor s, so the ratio h_{max}/h_{rms} is unchanged.

Figure 6 shows the cumulative probability for the ratio h_{max}/h_{rms} between the height of the highest asperity (relative to the average surface plane) and the rms roughness amplitude for the power spectra shown in Fig. 5 without (a) and with (b) a roll-off region. Note that for the case of no roll-off region the ratio h_{max}/h_{rms} is independent of the size of the surface area i.e. it is independent of the long-wavelength cut-off wavenumber q_0. For the case of a roll-off region the ratio h_{max}/h_{rms} increases continuously with increasing roll-off region $q_0 < q < q_r$.

We note that since h_{rms} is an average over the whole surface area it is nearly identical for all the 60 realizations so the finite width in the cumulative probabilities in Fig. 6 reflect the fluctuations in h_{max} and not in h_{rms}. This is illustrated in Fig. 7 which shows the cumulative probability distributions for h_{max} and h_{rms} for the system size $L = 2.53$ µm, but similar results occur for all the other studied system sizes. Note that $h_{rms} \approx 0.118$ µm for all the 60 realizations, with or without a roll-off region.

Figure 6 and 7 shows that the difference between the highest and lowest value of h_{max} is slightly larger than h_{rms} independent of the system size and the size of the roll-off region. Thus h_{max} for a given surface roughness realization is with ~ 90% probability in the range $\langle h_{max}\rangle \pm h_{rms}/2$, where $\langle h_{max}\rangle$ is the average of h_{max} over many realizations of the rough surface. In what follows, unless otherwise stated, h_{max} denote the average of $\langle h_{max}\rangle$ over all the 60 realizations used in the present study.

Figure 8 shows again the ratio h_{max}/h_{rms} for the power spectra shown in Fig. 5 ($H = 1$), and for similar power spectra for the Hurst exponent $H = 0.7$, as a function of the logarithm of the size of the unit L. Here h_{max}/h_{rms} is the average over all 60 realizations of the surface roughness $h(\mathbf{x})$. Note that for the case of no roll-off h_{max}/h_{rms} is independent of the system size L and hence independent of $q_0 = 2\pi/L$, while for the case of a roll-off h_{max}/h_{rms} increase nearly linearly with the logarithm of q_r/q_0. In the latter case the ratio h_{max}/h_{rms} will depend on the size L of the studied system as the roll-off region increases as $q_0 = 2\pi/L$ decreases.

We now discuss the results presented in Fig. 8 in more detail. First note that for a single surface roughness component

$$h(x) = h_{max}\cos(qx),$$

we get

$$h_{rms}^2 = \langle h^2\rangle = \frac{1}{L}\int_0^L \mathrm{d}x\, h_{rms}^2[\cos(qx)]^2 = \frac{1}{2}h_{max}^2,$$

so that $h_{max}/h_{rms} = \sqrt{2} \approx 1.414$.

Suppose now we have two roughness waves

$$h = h_A\cos(q_A x) + h_B\cos(q_B x).$$

In this case if integers n and m exist so that $q_A x = 2\pi n$ and $q_B x = 2\pi m$ then in at least one point x we have $h = h_A + h_B$ (constructive interference). This require $n/m = q_A/q_B$. If q_A/q_B is a rational number we can find integers n and m so that this equality is valid. In q_A/q_B is irrational number we can find integers so that the equality is satisfied to arbitrary accuracy. Hence we conclude that the function h will take as its maximum $h_A + h_B$ to an arbitrary good accuracy if the x interval (length L) is big enough. For large L the root-mean average

$$h_{rms}^2 = \frac{1}{L}\int_0^L \mathrm{d}x\, h^2$$
$$= \frac{1}{L}\int_0^L \mathrm{d}x\, \left[h_A\cos(q_A x) + h_B\cos(q_B x)\right]^2 \approx \frac{1}{2}\left(h_A^2 + h_B^2\right)$$

where we have used that the integral over x of the cross product term

$$2\cos(q_A x)\cos(q_B x) = \cos[(q_A + q_B)x] + \cos[(q_A - q_B)x]$$

gives a negligible contribution for large L. As an example if $h_A = h_B$ we get $h_{rms} = h_A$ while $h_{max} = 2h_A$ so that $h_{max}/h_{rms} = 2$. We note that adding even more roughness waves will increase h_{max} more than h_{rms} because in some locations on the surface the roughness waves will be nearly in phase and add together constructively resulting in a high asperity, while the same affect does not show up in h_{rms} as it is an average over the whole surface area.

All solids have surface roughness on many length scales and with wavevectors pointing in many directions, and the ratio h_{max}/h_{rms} will be larger than calculated for a single or two roughness components, as shown by the dashed lines in Fig. 8 which gives $h_{max}/h_{rms} \approx 2.5 - 3$ depending on the Hurst exponent. Now the reason for why h_{max}/h_{rms} does not increase with the system size when there is no roll-off region is due to the fact that in this case both h_{max} and h_{rms} are determined by the most long wavelength roughness components, which have the largest amplitude. Thus, the first few longest wavelength components with wavelength L, $L/2$, $L/3$, .. will determine both h_{max} and h_{rms}. This will not change as L increases and therefore h_{max} and h_{rms} will increase with the same factor as L increases, and h_{max}/h_{rms} remain independent of the system size L.

When the power spectrum has a roll-off region the situation is different as can be understood as follows. When a roll-off region occur there will be a range of long-wavelength roughness components (with wavenumber $q_0 < q < q_r$) with equal amplitudes. This follows from (7) which shows that the prefactor in front of each plane wave is the same as long as $C(\mathbf{q})$ is constant. When the roll-off region increases the number of these waves increases and at some points on the surface they may add with nearly equal phase (constructive interference) giving rise to a high asperity. This is similar to the occurrence of high (killer) waves on the ocean which occur with a finite but very small probability. At the same time h_{rms} does not increase very much as the roll-off region increase because the rms roughness integral (6) has a factor of q in it which reduces the small q contribution to the integral in the roll-off region where $C(\mathbf{q})$ is constant. In fact, if C_0 denote the constant value of $C(q)$ in the roll-off region then from (6) the contribution to h_{rms}^2 from the roll-off region is

$$\Delta h_{rms}^2 = \pi C_0 \left(q_r^2 - q_0^2\right),$$

which remain finite as $q_0 = 2\pi/L \to 0$ i.e. for an infinite system $L = \infty$. However an infinite system has a Gaussian distribution of surface heights which imply that there are arbitrary high asperities on the surface. Thus $h_{max}/h_{rms} \to \infty$ as the roll-off region L/λ_r becomes infinite large. In Appendix A we give an analytical expression for h_{max}/h_{rms} when a roll-off region occur.

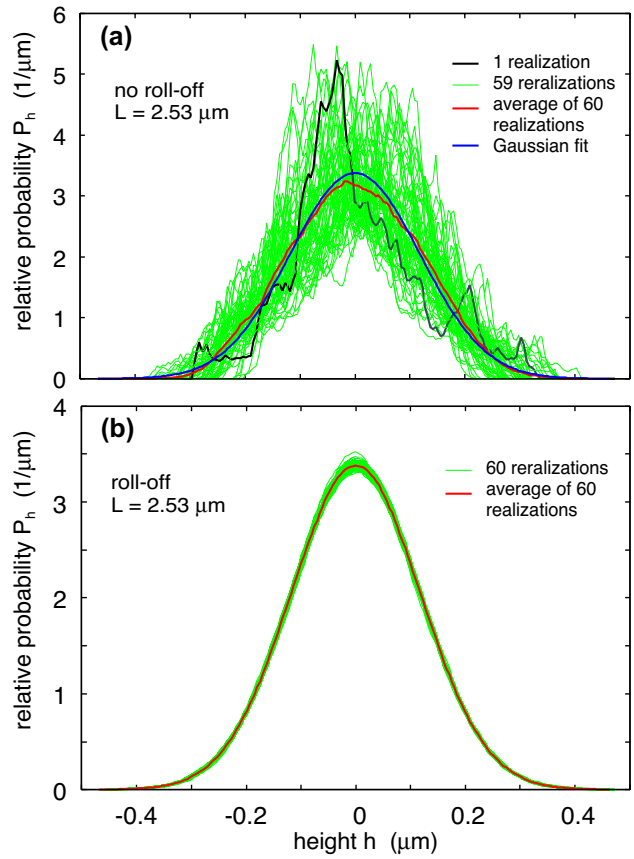

Fig. 9 The height probability distribution P_h as a function of the height as obtained from the computer simulations using 60 realizations of the roughness (green lines) for the case without (**a**) and with (**b**) a roll-off in the surface roughness power spectra. In **a** the black line shows P_h for one realization of the roughness. The red lines are the height distributions obtained by averaging over all the 60 realizations. The blue line in (**a**) is a Gaussian fit to the red line. In **b** we do not how the Gaussian fit as it would perfectly overlay the red line. The calculations are for a surface with $L = 2.53$ µm using the corresponding power spectra shown in Fig. 5a and b (Hurst exponent $H = 1$) (Color figure online)

We have stated above that for the case of no roll-off in the power spectrum the highest asperity (height h_{max}) and the rms roughness amplitude h_{rms} are determined by a few of the longest wavelength (and highest amplitude) roughness components. The phase of these roughness waves will differ in each realization of the surface roughness. This imply that the probability distribution of surface heights P_h, which depends mainly on the largest amplitude roughness components, will not be a Gaussian but will exhibit strong random fluctuations depending on the surface realization. This is illustrated in Fig. 9 which shows the height probability distribution P_h as a function of the height as obtained from the computer simulations using 60 realizations of the roughness

(green lines) for the case without (a) and with (b) a roll-off in the surface roughness power spectra. In (a) the black line shows P_h for one realization of the roughness, and is clearly very different from a Gaussian. The red lines are the height distributions obtained by averaging over all the 60 realizations. The blue line in (a) is a Gaussian fit to the red line. In (b) we do not how the Gaussian fit as it would perfectly overlay the red line. The calculations are for a surface with $L = 2.53$ µm using the corresponding power spectra shown in Fig. 5a and b (Hurst exponent $H = 1$).

For a randomly rough surface the depth $h_{\min}$ of the deepest valley will, when ensemble averaged, be the same as the height of the highest asperity, i.e. we expect for a given realization of a rough surface $h_{\max} \approx h_{\min}$. In the engineering community the difference between the tallest peak and the deepest valley is denoted by R_z, which we will denote h_z, and for a randomly rough surface it will equal $2h_{\max}$. Figure 8 shows that for typical Hurst exponents ($0.7 < H < 1$) if there is no roll-off in the power spectrum then $2h_{\max}/h_{\rm rms} \approx 5 - 6$. In most practical applications there is a roll-off in the power spectra typically extending over ~ 2 decades in length scale and in this case $2h_{\max}/h_{\rm rms} \approx 10$. The predicted range of h_z (between 5 and $10h_{\rm rms}$) is also observed for real surfaces in engineering applications [17].

We note that the roll-off region depends on the method of surface preparation. For example, if a surface is prepared using sand paper or a grinding wheel then the roll-off wavelength will be determined by the size of the particles which is determined by the grit number and typically range from $D \approx 20$ to 200 µm giving roll-off wavenumbers of order $q_{\rm r} = 2\pi/D \approx 3 \times 10^4 - 3 \times 10^5$ m^{-1}. If a surface is studied over a $L = 10$ mm region as typical in stylus measurements, then the the roll-off region (determined by the ratio L/D) could extend over 2 or 3 decades in length scale. However, in applications the effective region which matter may be much smaller, e.g., if a caliper is used to determine the width of a cylinder the "contact region" may be only $L \approx 0.1$ mm (see Appendix B), and in this case the roll-off region could be very small. It is clear that one must be very careful when performing topography measurements to probe surface areas of similar size as involved in the practical applications, or (better) one measure the topography over a bigger surface area but use only the relevant part of the surface roughness power spectrum.

4 Relation Between the Compression and the Contact Pressure

Let us first assume no surface roughness and denote the compression by δ. From the theory of elasticity the radial pressure acting at the interface $r = R_b$ is [4, 18]:

$$p = \frac{E^*\delta}{R_{\rm b}}, \tag{8}$$

where, if $\delta << R_{\rm b}$,

$$\frac{1}{E^*} = \frac{1}{2E_0}\left(\frac{R_{\rm c}^2 + R_{\rm b}^2}{R_{\rm c}^2 - R_{\rm b}^2} + \nu_0\right) + \frac{1}{2E_1}\left(\frac{R_{\rm b}^2 + R_{\rm a}^2}{R_{\rm b}^2 - R_{\rm a}^2} - \nu_1\right).$$

If both the outer and inner cylinder is of the same material with the Young's modulus E and Poison ratio ν we get

$$\frac{1}{E^*} = \frac{1}{E}\frac{R_{\rm b}^2(R_{\rm c}^2 - R_{\rm a}^2)}{(R_{\rm c}^2 - R_{\rm b}^2)(R_{\rm b}^2 - R_{\rm a}^2)}. \tag{9}$$

The compression δ is usually chosen so that the pressure p is below the plastic yield stress of the materials involved. As an example for steel $E \approx 2 \times 10^{11}$ Pa and assuming $R_{\rm a} = 0$, $R_{\rm b} = 0.5$ cm and $R_{\rm c} = 1$ cm and $p = 150$ MPa, which is typically half the yield stress of steel, we get from (8) and (9) $\delta = 10$ µm. This compression length is similar to the amplitude of the roughness in many cases. Since the roughness manifest itself as an elastically soft film on the steel surfaces one most take it into account in the analysis.

Contact mechanics theory [19] shows that the (elastic) contact between two solids with different surface roughness $h_0(\mathbf{x})$ and $h_1(\mathbf{x})$, and different elastic properties (Young's modulus E_0 and E_1, and Poisson ratio ν_0 and ν_1) can be mapped on a problem of the contact between an elastic half space (with the effective modulus $E_{\rm eff}$ and Poisson ratio $\nu = 0$) with a flat surface, and a rigid solid with the combined surface roughness $h(\mathbf{x}) = h_0(\mathbf{x}) + h_1(\mathbf{x})$. If the surface roughness on the two surfaces are uncorrelated then the surface roughness power spectrum of the rigid surface is the sum of the individual surface roughness:

$$C(\mathbf{q}) = C_0(\mathbf{q}) + C_1(\mathbf{q}),$$

where $C_0(\mathbf{q})$ and $C_1(\mathbf{q})$ are the power spectra of the original surfaces. This imply that the total mean square roughness obey

$$h_{\rm rms}^2 = h_{\rm rms0}^2 + h_{\rm rms1}^2.$$

The effective modulus of the elastic solid is determined by

$$\frac{1}{E_{\rm eff}} = \frac{1 - \nu_0^2}{E_0} + \frac{1 - \nu_1^2}{E_1}.$$

If both particles are made of the same material and produced the same way then $C(\mathbf{q}) = 2C_0(\mathbf{q})$ and $E_{\rm eff} = E_0/[2(1 - \nu_0^2)]$.

If the pressure p is not too height and not too small the Persson contact mechanics theory predict the following relation between the pressure p and the average surface separation u:

$$p = \beta E_{\text{eff}} e^{-u/u_0}, \tag{10}$$

where u_0 and β depends on the surface roughness power spectrum[1]. For a self affine fractal surface with the Hurst exponent $0.8 < H < 1$ we have [20] $u_0 \approx 0.5h_{\text{rms}}$. The parameter β depends on q_0, q_{r} and h_{rms} and for what is typical for grinded steel surfaces (see Fig. 2 in [9]), $h_{\text{rms}} = 2$ µm, $q_{\text{r}} = 10^5$ m^{-1} and $H = 0.8$ we get $\beta \approx 0.46$ when $q_0 = q_{\text{r}}$ (no roll-off region), $\beta \approx 0.17$ for $q_0 = 0.1q_{\text{r}}$ (one decade of roll-off region) and $\beta \approx 0.14$ when $q_0 = 0.01q_{\text{r}}$ (two decades of roll-off region). From (10) follows that

$$u = u_0 \ln\left(\beta \frac{E_{\text{eff}}}{p}\right),$$

or $u = \kappa h_{\text{rms}}$ with

$$\kappa \approx 0.5 \ln\left(\beta \frac{E_{\text{eff}}}{p}\right). \tag{11}$$

Using $E_{\text{eff}} = 0.5E/(1-\nu^2) \approx 10^{11}$ Pa and $p = 150$ MPa, we get $\kappa \approx 2.3$ and ≈ 2.4 with two and one decade of roll-off and 2.9 without a roll-off. Hence for the case of one decades of roll-off we predict that $\delta_{\text{eff}} = \delta_{\text{caliper}} - (h_{\max} - \kappa h_{\text{rms}}) \approx \delta_{\text{caliper}} - 1.6h_{\text{rms}}$ (where we have used the typical result expected when there are one decade of roll-off region $h_{\max} \approx 4h_{\text{rms}}$), which is similar to what have been suggested from analysis of experimental data (see Sec. 5). Still κ is not a constant but depends on the pressure and on the elastic properties of the solids, and $h_{\max}$ is not exactly $4h_{\text{rms}}$ but depends on the size L of the (caliber or micrometer screw gauge) contact region, and on the roll-off wavenumber q_{r} in the surface roughness power spectrum; $h_{\max} - \kappa h_{\text{rms}}$ decreases as the roll-off region decreases. We note that (11) is valid only if the pressure ratio p/E_{eff} is not too high or two low, and in the present case we are very close to the pressure where finite size effects are important [21]. For a more general case the $u(p)$ relation can be calculated using equations presented elsewhere [14, 15, 21, 22].

In the study above we have neglect plastic deformations. Plastic deformation may occur both on the asperity level [7, 8] and macroscopically [4, 5]. Plastic deformation will reduce the contact pressure and may result in changes in the macroscopic shape of the objects. For this reason press fits are usually designed to result in contact pressures below the macroscopic yield stress so that no macroscopic plastic deformation occurs. But even in such cases it is possible that plastic deformations occur on the asperity level as the contact stresses at high asperities may be much higher than the average or nominal contact pressure.

Plastic deformation of asperities for metals has been studied in several publications and is found to be smaller than expected based on the macroscopic yield stress. This could be due to work hardened surface layers but other explanations, based on plasticity mechanics of asperity interaction, has also been proposed [23–28]. Qualitatively, one may say that when an asperity becomes plastically deformed the stress field approach a hydrostatic stress and the asperity therefore becomes resistant to further plastic deformation. It is possible to model the influence of plasticity on asperity contact using simple flow models in boundary element calculations [7], or in the Persson contact mechanics approach using smoothing of the surfaces in wavevector space [8].

5 Discussion

In the engineering literature in the design of press fits the surface roughness of the contacting surfaces have been taken into account in an empirical way by reducing δ_{caliper} with a roughness dependent number. Thus, according to the DIN 7190 standard (see Ref. [6]) the effective compression to be used in calculations of the contact pressure $\delta_{\text{eff}} = \delta_{\text{caliper}} - b(h_{z0} + h_{z1})$ where $b = 0.4$. Assuming $h_z \approx 6h_{\text{rms}}$ (as expected if the roll-off region is small) this gives $\delta_{\text{eff}} \approx \delta_{\text{caliper}} - c(h_{\text{rms0}} + h_{\text{rms1}})$ where $c \approx 2.4$. For randomly rough surfaces, which have (when P_h is ensemble averaged) Gaussian height distributions, the arithmetic average roughness h_{a} can be related to the root mean square (rms) average $h_{\text{rms}} = \langle h^2 \rangle^{1/2}$ via $h_{\text{rms}} = (\pi/2)^{1/2} h_{\text{a}} \approx 1.25h_{\text{a}}$, which gives $\delta_{\text{eff}} \approx \delta_{\text{caliper}} - a(h_{\text{a0}} + h_{\text{a1}})$ where $a \approx 3$, as was also suggested in Ref. [3].

These empirical results are in rough agreement with the theory presented above, but the theory shows that the coefficient a (and b and c) depends on the contact pressure, the elastic properties of the solids, and on the surface roughness power spectrum. In particular, the extent of the roll-off region in the power spectrum is very important, and this depends on the size of the contact region used to probe the (inner and outer) diameter of the hub and shaft cylinders used in the press fit. If a caliper instrument is used this region is typically rectangular with the linear size of order $L \approx 0.3$ mm (see Appendix B), corresponding to a wavenumber $q_0 = 2\pi/L \approx 2 \times 10^4$ m^{-1}. A grinded steel surface has a typical roll-off wavenumber of 10^5 m^{-1} so the roll-off region in a typical case will be of order one decade in length scale. For this case

[1] Note that the parameter β is defined differently in Ref. [20]. In addition the parameter ε given in Ref. [20] was obtained for $\gamma = 1$ while for $\gamma = 0.4$ we get $\varepsilon = 4.047$. The numerical results in Ref. [20] are obtained for self-affine fractal power spectra without roll-off.

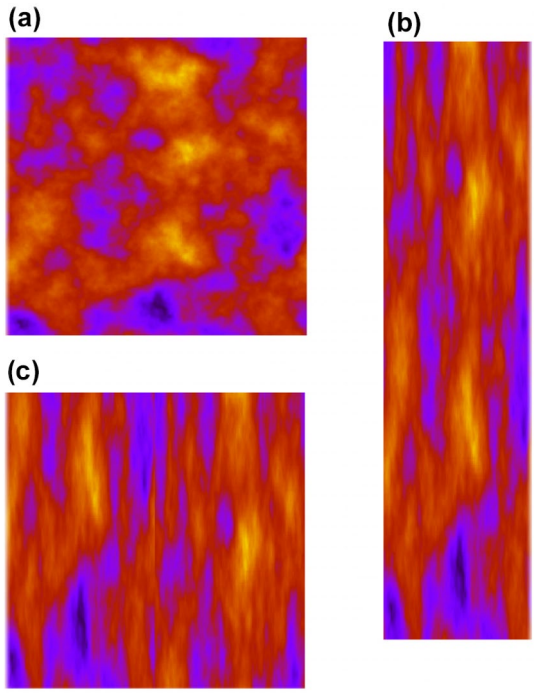

Fig. 10 **a** The height topography of a surface with isotropic roughness with the roll-off width $q_r/q_0 = 4$. **b** The same surface stretched by a factor of $\eta = 2$ in the y-direction and with $1/\eta = 0.5$ in the x-direction. This transformation result in a surface with the power spectrum $C(q_x\eta, q_y/\eta)$, where $C(q_x, q_y)$ is the power spectrum of the original surface. The anisotropic surface (**b**) has the same roll-off width in the x and y directions as the original surface (**a**) and the same ratio h_{max}/h_{rms}. **c** The elongated surface (**b**) is cut in η segments in the y-direction and joined together in the x-direction to form a square surface of the same size as the surface in (**a**) but with anisotropic roughness (color figure online)

from Fig. 8 we conclude that $h_{max} \approx 4h_{rms}$. In Sec. 4 we have showed that in a typical case $u \approx 2.4h_{rms}$ giving $\delta = \delta_{caliper} - (h_{max} - u) \approx \delta_{caliper} - 1.6h_{rms}$. The factor 1.6 is slighly smaller than the factor 2.4 expected from the empirical approch. Note that the roughness correction depends on $h_{rms} = (h_{rms0}^2 + h_{rms1}^2)^{1/2}$ and not on the sum $h_{rms0} + h_{rms1}$ as suggested in the empirical treatment. However, in many cases the roughness on one of the surfaces will dominate, and in these cases there is no big difference between these roughness amplitude factors.

In practice instead of using a caliper to measure the diameter of a cylinder, a micrometer screw gauge is often used as it has higher accuracy than a caliper (~ 1 µm, instead of ~ 10 µm as typical of caliper). The width of the contact region in the axial direction when using a micrometer screw may be larger than when using a caliper. Similarly, when measuring δ_{stylus} instead of using a stylus instrument, an optical method may be used as it is faster and may cover a rectangular strip rather than a line segment. However, our experience is that optical methods may not correctly (or accurately) describe the (small amplitude) short wavelength roughness, but this may be irrelevant for press fit applications as here the long wavelength (large amplitude) roughness is most important.

Since the maximum asperity height h_{max} is sensitive to rare surface defects it is not good to use it in a design criteria. Thus, instead of using the caliper compression one should use the stylus compression (as obtained by fitting the measured height profile to a circular segment).

In some applications the shaft and the hub surfaces, when averaged over the surface roughness (dashed line in Fig. 3), may not be perfectly cylindrical. This effect often referred to as cylindricity error, and will influence the contact pressure. This topic was addressed in Refs. [29, 30] and will not be considered here.

Most machined surfaces have anisotropic roughness, and may have different width of the roll-off regions in the x and y directions. It is interesting to study how the ratio h_{max}/h_{rms} depends on the width of roll-off regions in the x and y-directions for surfaces with anisotropic roughness. I will now argue that the results obtained for h_{max}/h_{rms} for isotropic roughness are still valid for anisotropic roughness if the effective roll-off width is defined as $q_r/q_0 = (\mu_x\mu_y)^{1/2}$, where μ_x is the roll-off width in the x-direction and μ_y is the roll-off width in the y-direction.

One way to generate anisotropic roughness mathematically is to stretch or contract a surface with isotropic roughness. This is illustrated in Fig. 10 where the original surface with isotropic roughness (a) is stretched in the y-direction with the factor $\eta = 2$ and contracted in the x-direction by the factor $1/\eta = 0.5$ resulting in the surface (b) with the same surface area but with anisotropic roughness. This correspond to scaling of the coordinates $x \to x' = x/\eta$ and $y \to y' = \eta y$. The power spectrum of the original surface $C(q_x, q_y)$ is transformed into $\tilde{C}(q_x, q_y) = C(q_x\eta, q_y/\eta)$. Note that the width $\mu = q_r/q_0$ of the roll-off region in both the x and y directions is unchanged by this transformation. Since the stretched surface consist of the same height values h as the original surface any functions of h (not depending on spatial derivatives of $h(\mathbf{x})$) will be unchanged, and in particular h_{max}/h_{rms} will be the same for the two surfaces in (a) and (b).

If the roll-off width is larger than η i.e. $q_r/q_0 > \eta$ then the elongated surface (b) can be "cut" in the y-direction in η segments and put together in the x-direction as to produce a square surface area [see Fig. 10c]. Such a surface would have the roll-off width $\mu_x = (q_r/q_0)\eta$ in the x-direction and $\mu_y = (q_r/q_0)/\eta$ in the y-direction. Note that $(\mu_x\mu_y)^{1/2} = q_r/q_0$ is equal to the roll-off width of the original surface with isotropic roughness.

Real anisotropic surfaces may not be accurately described as resulting from stretching of surfaces with isotropic

roughness but I believe the relation $q_r/q_0 = (\mu_x\mu_y)^{1/2}$ may hold in general.

For surfaces with anisotropic roughness, the average surface separation u, which enter in the compression $\delta_{\rm eff}$, can be obtained from the same equations as for isotropic roughness except that the power spectrum $C(q_x, q_y)$ must be replaced by its angular averaged value

$$C_{\rm av}(q) = \frac{1}{2\pi}\int_0^{2\pi} {\rm d}\theta\ C(q\cos\theta, q\sin\theta)$$

Finally we note that some surfaces of engineering interest are not (approximately) randomly rough. Thus, if a rough surface is exposed to (mild) wear it will smooth the upper part of the roughness profile resulting in a surface with negative skewness. Similarly, if hard cylinder with very smooth surface is rolling on a rough surface (roller burnishing) it will plastically deform the top of the asperities, again generating a surface profile with negative skewness [31]. And even the insertion process where the shaft is pushed into the hub will result in a smoothing of the highest asperities [32]. This effect is reduced in shrink fits. In all these cases the numerical results presented in Figs. 6 and 8 will be quantitatively modified, but the qualitative picture does not change.

6 Summary and Conclusion

A press fit, also known as interfererence fit or friction fit, is a form of fastening between two tight fitting mating parts that produces a joint which is held together by friction after the parts are pushed together. I have discussed the influence of surface roughness on the design of press fits. In the engineering community the diameter of the cylinders to be joined are usually determined using a caliper or micrometer screw. The diameter obtained this way depends on the height of the biggest asperities in the caliper-cylinder contact region. But the maximum asperity height $h_{\rm max}$ is sensitive to rare surface defects, and even for perfect systems there are relative large fluctuations in $h_{\rm max}$ between different realizations of the surface (see Fig. 6). Hence using the caliper-based compression is not a well defined way to include the surface roughness in calculating the contact pressure. We suggest that one instead use the stylus-based compression as obtained from fitting the measured height profile to a circular segment.

I have presented a detailed study of some important aspects of surface roughness, of interest in its own right, and shown how the surface roughness can be included when predicting the contact pressure in press fit. In this study I have neglected plastic deformations but for metals this can be included approximately on both the asperity level and on the macroscopic level using results presented elsewhere.

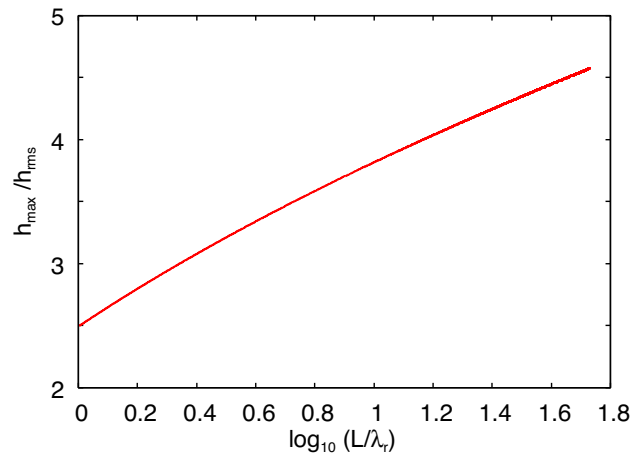

Fig. 11 The ratio $h_{\rm max}/h_{\rm rms}$ as a function of the logarithm of the size of the roll-off region L/λ_r where λ_r is the roll-off wavelength which is also the size L_0 of the self-affine fractal part of the studied unit. The result is obtained from (A3) using $N = N_0 \times (L/\lambda_r)^2$ where $\lambda_r = L_0 = 0.08$ μm and $N_0 = 140$

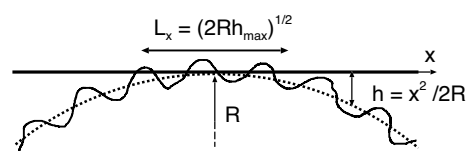

Fig. 12 A cylinder with surface roughness in contact with a flat surface. The effective contact width in the angular direction $L_x \approx (2Rh_{\rm max})^{1/2}$ where $h_{\rm max}$ is the height of the highest asperity in the effective contact area

Appendix A: $h_{\rm max}/h_{\rm rms}$ with Roll-Off Region

Here we show why $h_{\rm max}$ increases with the size of the roll-off region. First note that for an infinite system the height probability distribution is a Gaussian

$$P(h) = \frac{1}{(2\pi)^{1/2}h_{\rm rms}} e^{-(h/h_{\rm rms})^2/2}, \tag{A1}$$

which imply that there will be arbitrary high asperities at some points. However, for any finite system the probability to find very high asperities is small. For a surface with a roll-off region in the power spectrum there will be a natural (or characteristic) length determined by the roll-off wavenumber via $\lambda_r = 2\pi/q_r$. We can imagine the surface to be divided into $N = (L/\lambda_r)^2$ repeated but uncorrelated units. This imply that there will be roughly $N = N_0 \times (L/\lambda_r)^2$ uncorrelated points on the surface, where we choose N_0 so that $h_{\rm max}/h_{\rm rms}$ takes it correct value for the case of no roll-off where $L/\lambda_r = 1$. The height $h_{\rm max}$ can be obtained from the condition

$$\int_{h_{\max}}^{\infty} \mathrm{d}h\, P(h) \approx N^{-1}. \tag{A2}$$

Denoting $x = h_{\max}/h_{\mathrm{rms}}$ from (A1) and (A2) we get if $N >> 1$:

$$x \approx \left[2\ln\left(\frac{N}{(2\pi)^{1/2}x}\right)\right]^{1/2}. \tag{A3}$$

Using $N_0 = 140$ and increasing N continuously from N_0 to $N_0 \times (L/\lambda_{\mathrm{r}})^2 \approx N_0 \times 4000$ (where we have used $\lambda_{\mathrm{r}} = 0.08$ µm and $L = 5.06$ µm as in Fig. 8) gives the result shown in Fig. 11 which is virtually identical to the curve in Fig. 8 for $H = 1$ (with roll-off).

Appendix B: Effective Contact Area

Consider a flat surface in contact with a cylinder along the line $x = 0$ in a xy-coordinate system located in the flat surface (see Fig. 12). We assume the contact force is negligible so elastic deformations can be neglected, as expected when using a caliper to measure the cylinder diameter. If the cylinder (radius R) is perfectly smooth then the separation between the flat and the cylinder in the angular x-direction for $|x| << R$ is $h \approx x^2/(2R)$. For a cylinder with surface roughness if $h_{\max}$ is the height of an asperity it will make contact with the flat if it is located at $|x| < (2Rh_{\max})^{1/2}$. This imply that the effective size of the contact area in the x-direction is $L_x \approx (2Rh_{\max})^{1/2}$. For a cylinder with $R = 1$ cm and assuming $h_{\max} = 5$ µm we get $L_x \approx 0.3$ mm. The width of the contact area in the axial y-direction depends on the actual system considered. Thus for a caliper the width in the y-direction is determined by the width of the caliper metal blade which contact the cylinder and which typically is $L_y = 0.1 - 0.3$ mm.

Acknowledgements I thank W.G. Sawyer for pointing out the importance of surface roughness in head-stem taper junctions for hip implants, and N. Spencer for pointing out that press fits cannot be used for materials (like polymers) which exhibit creep. I thank A. Almqvist for comments on the text.

Author contributions I am alone author and everything presented has been obtained by me

Funding Open Access funding enabled and organized by Projekt DEAL. Open Access funding enabled and organized by Projekt DEAL. The authors have not disclosed any funding.

Declarations

Conflict of interest The author declare no conflict of interest in this study.

Open Access This article is licensed under a Creative Commons Attribution 4.0 International License, which permits use, sharing, adaptation, distribution and reproduction in any medium or format, as long as you give appropriate credit to the original author(s) and the source, provide a link to the Creative Commons licence, and indicate if changes were made. The images or other third party material in this article are included in the article's Creative Commons licence, unless indicated otherwise in a credit line to the material. If material is not included in the article's Creative Commons licence and your intended use is not permitted by statutory regulation or exceeds the permitted use, you will need to obtain permission directly from the copyright holder. To view a copy of this licence, visit http://creativecommons.org/licenses/by/4.0/.

References

1. Gustafson, J.A., Mell, S.P., Levine, B.R., Pourzal, R., Lundberg, H.J.: Interaction of surface topography and taper mismatch on head-stem modular junction contact mechanics during assembly in modern total hip replacement, J. Orthop. Res. (2022) https://doi.org/10.1002/jor.25357
2. Stockhausen, K.E., Riedel, C., Belinski, A.V., Rothe, D., Gehrke, T., Klebig, F., Gebauer, M., Amling, M., Citak, M., Busse, B.: Variability in stem taper surface topography affects the degree of corrosion and fretting in total hip arthroplasty. Sci. Rep. **11**, 9348 (2011)
3. Loc, N.H., Phong, L.V.: Study of interference fit between steel and brass parts. EUREKA **5**, 140 (2022). https://doi.org/10.21303/2461-4262.2022.002524
4. Madej, J., Sliwka, M.: Analysis of interference-fit joints. Appl. Sci. **11**, 11428 (2021)
5. Maxim, D.I.: The effect of manufacturing on the press fit insertation force. IOP Conf. Ser. **416**, 012050 (2018)
6. DIN 7190.: (2017), Interference fits - Calculation and design rules. DIN 7190 (2001) proposed a reduction of effective interference by $0.8R_z$, which was reduced to $0.4R_z$ in DIN 7190 (2017)
7. Tiwari, A., Almqvist, A., Persson, B.N.J.: Plastic deformation of rough metallic surfaces. Tribol. Lett. **68**, 1 (2020)
8. Fischer, F.J., Schmitz, K., Tiwari, A., Persson, B.N.J.: Fluid leakage in metallic seals. Tribol. Lett. **68**, 1 (2020)
9. Persson, B.N.J.: On the fractal dimension of rough surfaces. Tribol. Lett. **54**, 99 (2014)
10. Nayak, P.R.: Random process model of rough surfaces. J. Lubr. Technol. **93**, 398 (1971)
11. Carbone, G., Lorenz, B., Persson, B.N.J., Wohlers, A.: Contact mechanics and rubber friction for randomly rough surfaces with anisotropic statistical properties. Eur. Phys. J. E **29**, 275 (2009)
12. Jacobs, T.D.B., Junge, T., Pastewka, L.: Quantitative characterization of surface topography using spectral analysis. Surf. Topogr. **5**, 013001 (2017)
13. Persson, B.N.J.: Theory of rubber friction and contact mechanics. J. Chem. Phys. **115**, 3840 (2001)
14. Almqvist, A., Campana, C., Prodanov, N., Persson, B.N.J.: Interfacial separation between elastic solids with randomly rough surfaces: comparison between theory and numerical techniques. J. Mech. Phys. Solids **59**, 2355 (2012)
15. Afferrante, L., Bottiglione, F., Putignano, C., Persson, B.N.J., Carbone, G.: Elastic contact mechanics of randomly rough surfaces: an assessment of advanced asperity models and Persson's theory. Tribol. Lett. **66**, 1 (2018)
16. Persson, B.N.J., Albohr, O., Tartaglino, U., Volokitin, A.I., Tosatti, E.: On the nature of surface roughness with application to contact mechanics, sealing, rubber friction and adhesion. J. Phys. **17**, R1 (2004)

17. Schmidt, J., Thorenz, B., Schreiner, F., Döpper, F.: Comparison of areal and profile surface measurement methods for evaluating surface properties of machined components. Procedia CIRP **102**, 495 (2021)
18. Schmid, S.R., Hamrock, B.J., Jacobson, B.: Fundamentals of Machine Elements. CRC Press, New York (2014)
19. Johnson, K.L.: Contact Mechanics. Cambridge University Press, Cambridge (1985)
20. Persson, B.N.J.: Relation between interfacial separation and load: a general theory of contact mechanics. Phys. Rev. Lett. **99**, 125502 (2007)
21. Pastewka, L., Prodanov, N., Lorenz, B., Müser, M.H., Robbins, M.O., Persson, B.N.J.: Finite-size scaling in the interfacial stiffness of rough elastic contacts. Phys. Rev. E **87**, 062809 (2013)
22. Yang, C., Persson, B.N.J.: Contact mechanics: contact area and interfacial separation from small contact to full contact. J. Phys. **20**, 215214 (2008)
23. Williamson, J.B.P., Hunt, R.T.: Asperity persistence and the real area of contact between rough surfaces. Proc. R. Soc. Lond. A **327**(1569), 147 (1972)
24. Childs, T.H.C.: The persistence of roughness between surfaces in static contact. Proc. R. Soc. Lond. A **353**, 35 (1977)
25. Childs, T.H.C.: The persistence of asperities in indentation experiments. Wear **25**, 3 (1973)
26. Broitman, E.: Indentation hardness measurements at macro-micro- and nanoscale: a critical overview. Tribol. Lett. **65**, 23 (2017)
27. Wang, X., An, B., Xu, Y., Jackson, R.L.: The effect of resolution on the deterministic finite element elastic-plastic rough surface contact under combined normal and tangential loading. Tribol. Int. **144**, 106141 (2020)
28. Manners, W.: Plastic deformation of a sinusoidal surface. Wear **264**, 60 (2008)
29. Raj, A.P., Bhatti, A., Dhanish, P.B.: Combined effect of cylindricity, roundness and roughness on axial load-carrying ability of interference fits. Proc. Inst. Mech. Eng. Part J **234**, 1697 (2020)
30. Wang, C.P., Qi, H.Y., Hao, W.X., Hou, D.M.: Three-dimensional contact surface modeling and stress analysis of interference fit based on cylindricity error. Archive Appl. Mech. **92**, 993 (2022)
31. Perez-Rafols, F., Almqvist, A., 0: On the stiffness of surfaces with non-Gaussian height distribution. Sci. Rep. **11**, 1863 (2021)
32. Ramachandran, R.V., Radhakrishnan, R.: Influence of surface finish in interference fits. Int. J. Product. Res. **12**, 705 (1974)

Publisher's Note Springer Nature remains neutral with regard to jurisdictional claims in published maps and institutional affiliations.